ADVANCES IN ATMOSPHERIC SCIENCES, VOL. 24, NO. 3, 2007, 343–359

Time-Frequency Characteristics of the Relationships Between Tropical Indo-Pacific SSTs

Song YANG*[1], DING Xiaoli[2] (丁晓利), ZHENG Dawei[3] (郑大伟), and Soo-Hyun YOO[4]

[1] *NOAA's Climate Prediction Center,* 5200 *Auth Road, Camp Springs, MD* 20746*, USA*

[2] *Department of Land Surveying and Geo-Informatics, Hong Kong Polytechnic University*

[3] *Center for Astrogeodynamics Research, Shanghai Astronomical Observatory,*

Chinese Academy of Sciences, Shanghai 200030

[4] *RSIS/Climate Prediction Center,* 5200 *Auth Road, Camp Springs, MD* 20746*, USA*

(Received 14 August 2005; revised 18 September 2006)

ABSTRACT

In this study, several advanced analysis methods are applied to understand the relationships between the Niño-3.4 sea surface temperatures (SST) and the SSTs related to the tropical Indian Ocean Dipole (IOD). By analyzing a long data record, the authors focus on the time-frequency characteristics of these relationships, and of the structure of IOD. They also focus on the seasonal dependence of those characteristics in both time and frequency domains.

Among the Niño-3.4 SST, IOD, and SSTs over the tropical western Indian Ocean (WIO) and eastern Indian Ocean (EIO), the WIO SST has the strongest annual and semiannual oscillations. While the Niño-3.4 SST has large inter-annual variability that is only second to its annual variability, the IOD is characterized by the largest semiannual oscillation, which is even stronger than its annual oscillation. The IOD is strongly and stably related to the EIO SST in a wide range of frequency bands and in all seasons. However, it is less significantly related to the WIO SST in the boreal winter and spring. There exists a generally weak and unstable relationship between the WIO and EIO SSTs, especially in the biennial and higher frequency bands. The relationship is especially weak in summer and fall, when IOD is apparent, but appears highly positive in winter and spring, when the IOD is unimportantly weak and even disappears. This feature reflects a caution in the definition and application of IOD. The Niño-3.4 SST has a strong positive relationship with the WIO SST in all seasons, mainly in the biennial and longer frequency bands. However, it shows no significant relationship with the EIO SST in summer and fall, and with IOD in winter and spring.

Key words: Indian Ocean dipole, ENSO, time-frequency relationship, coherence analysis

DOI: 10.1007/s00376-007-0343-z

1. Introduction

The El Niño Southern Oscillation (ENSO) and the Indian Ocean dipole (IOD) have been considered two important phenomena that affect the climate in Africa, Asia, and Australia and over the Indo-Pacific oceans. Since the 1982/83 El Niño event, it has been realized that ENSO is perhaps the most important phenomenon that causes anomalies in global climate on inter-annual timescales (Rasmusson and Carpenter, 1982; Ropelewski and Halpert, 1987; and Yulaeva and Wallace, 1994). For example, substantial evidence has demonstrated that ENSO regulates strongly the variability of the Asian-Australian monsoon system (Rasmusson and Carpenter, 1983; Webster and Yang, 1992; Ju and Slingo, 1995; Gadgil and Sajani, 1998; Zhang et al., 1999; Wang et al., 2000; Ailikun and Yasunari, 2001; Lau and Wu, 2001; Huang et al., 2004; and see review in Lau and Wang, 2006; and Yang and Lau, 2006). Recently, a zonal dipole mode has been spotted in the tropical Indian Ocean (IO; Saji et al., 1999; Webster et al., 1999), referred to as IOD here, and it

*Song.Yang@noaa.gov

is believed to account for many climate anomalies in Africa, Asia, and Australia (Li and Mu, 2001a; Ashok et al., 2003a; Guan and Yamagata, 2003; Saji and Yamagata, 2003a; Black, 2005; Rao and Behera, 2005; Saji et al., 2005; Yang and Li, 2005). Several studies have even linked IOD to the climate anomalies in Europe and the Americas (Li and Mu, 2001b; Saji and Yamagata, 2003a; Saji et al., 2005).

Because of the large climate impacts of ENSO and IOD, the relationship between the two phenomena has been a subject of extensive interest during recent years. In their original work on IOD, Saji et al. (1999) and Webster et al. (1999) declared that the variability of IOD is independent from that of ENSO (see also Behera et al., 1999). Ashok et al. (2001) also showed that whenever the relationship between the Indian monsoon and ENSO is low, the relationship between the monsoon and IOD is high, and vice versa. Loschnigg et al. (2003) claimed that the IOD is an inherent feature of the Asian monsoon and tropospheric biennial oscillation (TBO). Saji and Yamagata (2003b) further argued that the IOD arises from the inherent coupled air-sea interaction in the tropical Indian Ocean (IO) and is not a part of ENSO evolution.

On the other hand, other studies have indicated that the variability of IOD and ENSO is not independent from each other. It has been shown that variations of IOD and ENSO, both of which are linked to the overlying Walker-type atmospheric circulation (Chao et al., 2005), are closely related to each other (Huang and Kinter III, 2002; Li et al., 2002a; Li et al., 2002b) and that both phenomena are associated with African rainfall in the same phase (Black et al., 2003). It is argued that the IOD and ENSO, which are related to each other most strongly in fall, are two interactive phenomena (e.g., Yoo et al., 2006; Zhang and Yang, 2007). In spite of their distinctive evolution characteristics, they are dynamically coupled ocean-atmosphere modes linked to the annual cycle of the basic state (Li et al., 2003; Yu et al., 2003) and are often the large-amplitude excursions of TBO over the tropical Indo-Pacific oceans (Meehl et al., 2003). Li et al. (2003) indicated that ENSO is one of the triggering mechanisms for IOD and attributed the biennial tendency of IOD to ENSO forcing. In addition, several studies have shown that the variations of IOD lead those of ENSO (e.g., Behera and Yamagata, 2003 and that IOD influences the intensity and frequency of ENSO (Wu and Kirtman, 2004) and even modifies the impact of El Niño on the Indian monsoon (Ashok et al., 2004).

While whether the ENSO and IOD related sea surface temperatures (SSTs) are independent from each other is still under much debate, one should assume that the variability of the two phenomena is independent from each other during some periods of time and on some timescales, but not independent during other time periods and on other timescales. In any case, the details of the relationship between the two phenomena have not fully surfaced. In this study, we apply several advanced analysis methods to understand the detailed features of the structure of IOD and the relationship between ENSO and IOD-related SSTs in time and frequency domains. We focus on the Niño-3.4 SST, IOD, and the SSTs over the tropical western Indian Ocean (WIO) and eastern Indian Ocean (EIO). We also focus on the seasonality of the time-frequency characteristics of the various phenomena or SSTs. The analysis is aimed at providing useful information about the dependence or independence between ENSO and IOD.

In section 2, the data set and analysis methods are described briefly. In sections 3 and 4, the time-frequency characteristics of the variability of tropical Indo-Pacific SSTs and of the relationship between the SSTs are discussed, respectively. We further discuss the seasonality of these SST characteristics in section 5 and summarize the results of the study in section 6.

2. Data and analysis methods

2.1 *Data*

The data analyzed in this study is mainly from the National Oceanic and Atmospheric Adminstration (NOAA) Extended Reconstructed SST (ERSST; Smith and Reynolds, 2003) dataset. The ERSST, which is available monthly and has been applied widely in climate study, covers an extended period since 1800. Here, we analyze the data from January 1880 to December 2004 because the data for the early decades are not reliable (e.g., Yan et al., 2003). We analyze the SSTs averaged over the Niño-3.4 region (5°N–5°S, 170°–110°W), tropical WIO (10°S–10°N, 50°–70°E), and tropical EIO (10°S–0°, 90°–110°E). Following Saji et al. (1999), we define IOD as the difference in SST between WIO and EIO (WIO SST minus EIO SST).

2.2 *Methods of analysis*

We apply several advanced analysis tools to understand the features of the variability of different SST indices. We first apply the techniques of wavelet analysis and least squares method to depict the time-frequency features and the dominant oscillating timescales of the indices. For the relationships between the different indices, we analyze the features of their coherence, lead-lag correlation, and seasonality. In particular, we focus on the characteristic features of the relationships between different SSTs in both time and frequency domains, by applying a recently developed technique in which a multiple moving window method is used. De-

tails of these analyses tools, which have been applied by Ding et al. (2002) for temperature and by Yang et al. (2007) for precipitation analysis, will be discussed in sections 3–5 correspondingly.

3. Time-frequency characteristics of the variability of tropical Indo-Pacific SSTs

In this section, we apply wavelet transform (Morlet et al., 1982) and the least squares method of Householder transform (see Powell and Reid, 1969) to illustrate the time-frequency characteristics of IOD and Niño-3.4, WIO, and EIO SSTs. For a time series $f(t)$, the wavelet transform is defined as:

$$W_\psi(f)(a,b) = \frac{1}{\sqrt{a}} \int_{-\infty}^{\infty} f(t)\psi\left(\frac{t-b}{a}\right) dt\,. \quad (1)$$

where $\psi(t)$ is the basic wavelet, a the dilation/compression scale factor defining the characteristic frequency, and b the translational factor in the time domain. One of the known advantages of the wavelet transform is that it can describe the spectral characteristics of time series $f(t)$ in the time-frequency domain (the $a-b$ space with horizontal time axis b and vertical frequency axis a). In other words, the changes in the signals of a specific data series can be displayed simultaneously in the time-frequency domain and the spectral distributions of the signals in different frequencies visualized over the same time span. However, distorted edge effect of wavelet spectrum may occur in the transform, especially in the lower frequency bands. For this reason, we apply the leap-step time series analysis (LSTSA) model developed by Zheng et al. (2000), which improves the data information of end points in wavelet analysis and effectively reduces the edge effects of the filtered output signals. The LSTSA is a nonlinear model decomposing a time series into deterministic and stochastic components, in which the stochastic component is further characterized by several stochastic models and each stochastic model is valid within a sub-domain of the time series (leap-step domain). It provides greater stability for long-range forecasting. The main features of the LSTSA model have also been summarized in the Appendix of Yang et al. (2007).

Figure 1 displays the wavelet spectrum of various monthly SST indices for the period of 1880–2004. It shows amplitude spectra, instead of power spectra, for a better display of the signals. The Niño-3.4 SST has a strong annual cycle and large lower-frequency variability on timescales of 2–7 years (Fig. 1a). However, semiannual signals are not apparent in Niño-3.4 SST. On the other hand, semiannual signals occur clearly in both IOD and WIO SST (Figs. 1b and c). In fact, the semiannual signal dominates over the signals of all timescales for IOD. It can be seen from Figs. 1b–d that annual oscillation is apparent in all IO SSTs, especially in the WIO SST. For EIO SST, the annual oscillation clearly dominates over the signals of all other timescales. However, inter-annual and longer variability appears only moderately in IOD and EIO SST, and is even weaker in WIO SST. The relatively large inter-annual variability (on timescales 3–5 years) of IOD in the 1960s and 1990s (Fig. 1b) is consistent with the results of Saji and Yamagata (2003b) in their analysis for the period of 1958–97.

After identifying the dominant timescales of the SST indices, largely qualitatively, by wavelet analysis, we further quantitatively determine the mean magnitudes and phases of the temporal variations of SST by applying a least-square method, which enables an estimation of stable parameters. Our focus is on the features of annual, semiannual, inter-annual, and inter-decadal timescales, although we will also compute the constant and linear trend terms. Although the "first guess" from Fig. 1 is not necessary for the least-square analysis, it provides great efficiency to our experimental computations. The least-square method of Householder transform, which is a linear regression problem, is given as follows:

$$L_t = a + bt + \sum_{k=1}^{7} c_k \sin(2\pi t/P_k + \varphi_k) + \varepsilon_t\,. \quad (2)$$

where P_k, c_k, and φ_k are, respectively, the periods, amplitudes, and phases of the annual, semiannual, inter-annual, and inter-decadal terms, and a and b are the constant and linear terms. ε_t is the white noise at time t. Since the periods of inter-annual and inter-decadal fluctuations are relatively unstable and drifts in frequency may occur in the spectral estimate (see Fig. 1), we determine their mean values by a method of trial and error in the process of least squares computations. Specifically, we identify and determine the optimal mean periods of the spectral signals by adjusting the periodic values step by step. In this process, the amplitudes and phases of the spectral signals are also estimated and the uncertainties in period of the signals are measured by the standard deviations of phases.

Table 1 shows the information estimated for the seven most dominant terms (annual, semiannual, three inter-annual terms, and two inter-decadal terms) from Eq. (2) for the four Indo-Pacific SST indices, respectively. The periods are identified by the means of least-square adjustment of Householder transform, and the phase estimation is referenced to the epoch of January 1880, the beginning epoch of the data series. The Niño-3.4 SST has largest amplitudes on the annual

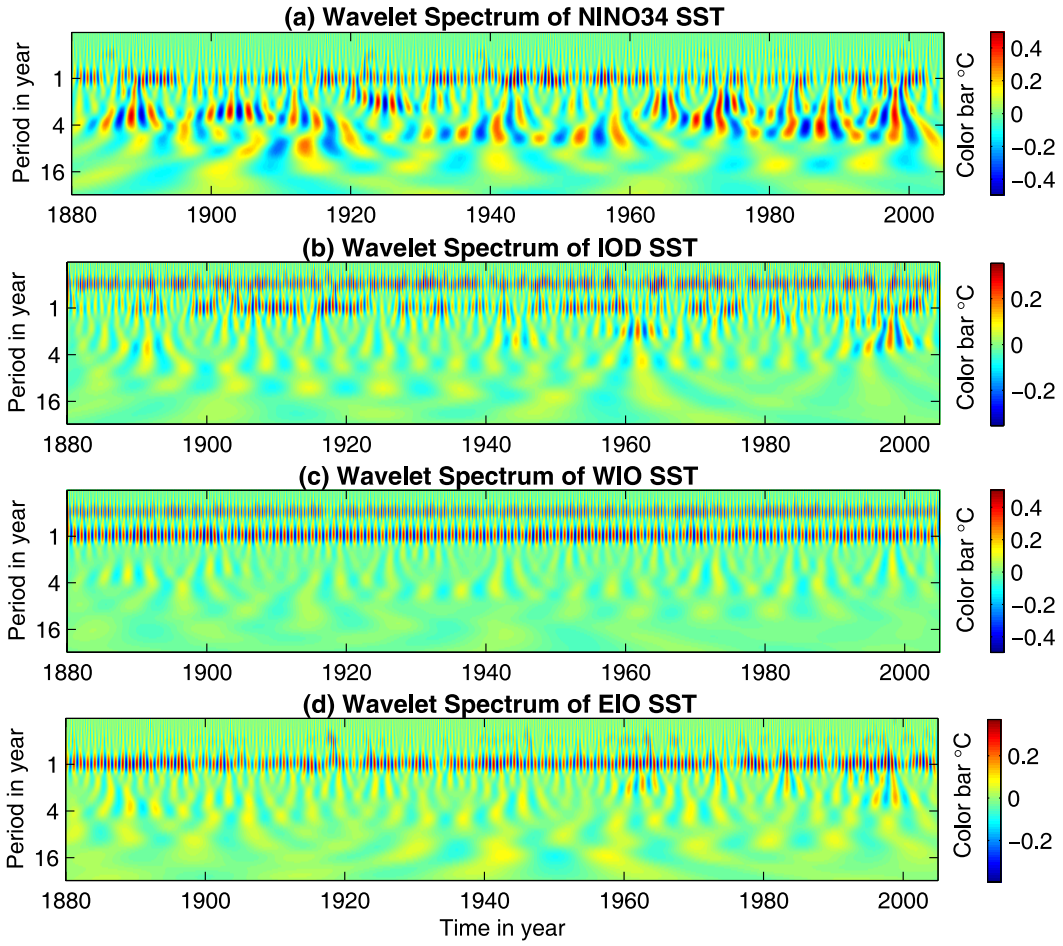

Fig. 1. Wavelet spectra of monthly (a) Niño-3.4 SST, (b) IOD, (c) WIO SST, and (d) EIO SST, for the period from January 1880 to December 2004. The red and blue colors represent the largest positive and negative amplitudes of wavelet spectra, respectively. The y-coordinate represents the periodic timescales of the time-frequency spectra.

timescale (row eight of the upper left portion) and inter-annual timescale of 5.6 years: 0.61°C and 0.30°C, respectively. It also fluctuates apparently on the timescales of 3.5 years, 13.2 years, and 6 months (semi-annual timescale). On the other hand, the IOD has a larger amplitude on the semiannual timescale (0.47°C) than on the annual timescale (0.35°C), which is different from the WIO and EIO SSTs, both of which have the largest amplitude on the annual timescale and the second largest amplitude on the semiannual timescale (see the lower portion of the table). The annual signal and semiannual signal are 0.81°C and 0.62°C for WIO and 0.56°C and 0.21°C for EIO. In all IO SST indices, the nonseasonal signals are smaller than those of the annual and semiannual timescales by an order of magnitude. This feature marks a significant difference between the Indian Ocean and Pacific SSTs. Also, In the IO, the largest amplitude of both annual and semiannual signals appears in WIO, and the weakest annual oscillation and semiannual oscillation appear in IOD and in EIO respectively.

Table 1 also shows several other major features. First, the most dominant oscillating timescales are also the timescales of the most stable estimations of phase. This is especially apparent in the annual and semiannual oscillations of WIO SST, as seen in the values of standard deviation of 22.0±0.7 and -119.3 ± 0.9 (column three and rows eight and nine of the upper left portion). Second, there exist warming trends in all SST indices, with the largest in WIO SST (0.73°C per 100 years) and smallest in IOD (0.21°C per 100 years).

The values of root-mean-square (RMS) in Table 1 weigh the importance of the SST variability of the selected oscillating timescales and the constant and linear terms, relative to the total SST variability. For each SST time series, they are calculated respectively from the original time series (inside the parentheses; e.g. 0.952°C for Niño-3.4 SST) and from the residual

Table 1. Estimations of the parameters of oscillating signals detected in the monthly data series of Niño-3.4 SST, IOD, and WIO and EIO SSTs from January 1880 to December 2004.

	Period (yr)	Amplitude (°C)	Phase (°)	Linear rate (°C yr^{-1})	RMS
Niño-3.4 SST	21.0	0.156±0.027	−18.5 ± 10.0	0.0040±0.0005	0.741 (0.952, 22%)
	13.2	0.255±0.027	−102.0 ± 6.1		
	5.6	0.302±0.027	−145.5 ± 5.1		
	3.5	0.263±0.027	−33.4 ± 5.9		
	2.1	0.138±0.027	80.3±11.2		
	1.0	0.608±0.027	−29.3 ± 2.6		
	0.5	0.214±0.027	−132.8 ± 7.3		
IOD SST	23.8	0.062±0.013	155.9±11.5	0.0021±0.0002	0.343 (0.551, 38%)
	11.5	0.053±0.013	−136.5 ± 13.5		
	5.4	0.086±0.013	115.0±8.3		
	3.6	0.053±0.013	−42.7±13.5		
	2.0	0.072±0.013	140.6±10.0		
	1.0	0.347±0.013	56.5±2.1		
	0.5	0.472±0.013	−104.6 ± 1.5		
WIO SST	19.6	0.068±0.010	71.2±8.2	0.0073±0.0002	0.263 (0.816, 68%)
	10.8	0.044±0.010	−0.6 ± 12.6		
	5.1	0.087±0.010	−135.9 ± 6.3		
	3.5	0.058±0.010	−52.4 ± 9.5		
	2.0	0.031±0.010	171.2±18.0		
	1.0	0.809±0.010	22.0±0.7		
	0.5	0.622±0.010	−119.3 ± 0.9		
EIO SST	19.6	0.049±0.012	90.8±13.8	0.0052±0.0002	0.322 (0.566, 43%)
	11.8	0.049±0.012	6.7±13.8		
	5.5	0.049±0.012	−102.8 ± 13.8		
	3.5	0.050±0.012	−81.4 ± 13.4		
	2.1	0.049±0.012	10.2±13.7		
	1.0	0.559±0.012	1.3±1.2		
	0.5	0.208±0.012	−155.1 ± 3.2		

series after the seven oscillating signals and the constant and linear trend terms are removed from the original SST data (outside the parentheses; e.g. 0.741°C for Niño-3.4 SST). It is seen that the oscillating timescales and the constant and linear terms (mainly the annual and semiannual signals) account for a major portion [68%, calculated as $(0.816 - 0.263)/0.816$] of the total SST variability in WIO. On the other hand, the contribution of the frequency-oscillating signals and the constant and linear terms detected by the wavelet spectra to the total SST RMS is only 22% in the Niño-3.4 region. The IOD (38%) and the EIO SST (43%) go between the WIO and Niño-3.4 SSTs.

4. Time-frequency characteristics of the coherence between various SST indices

After depicting the features of dominant timescales of the variations of Indo-Pacific SSTs, we investigate the time-frequency characteristics of the interrelationships between these SSTs. To examine the relationship between two specific fields, we analyze the cross-correlation function and the squared coherence spectrum. To illustrate the time-frequency characteristics of the coherence, as in Yang et al. (2007), we apply a moving window technique in which we first estimate the values of coherence for a sub-series of ten years and then move successively the data points for subsequent estimations.

As in Jenkins and Watts (1968), the cross-correlation function $\rho(\tau)$ in the time domain and the squared coherence spectrum $\gamma^2(f)$ in the frequency domain between any given two time series are computed as:

$$\rho(\tau) = \sigma_{12}(\tau)/(\sigma_{11}\sigma_{22})^{1/2} \tag{3}$$

$$R(f) = S_{12}(f)/(S_{11}(f)S_{22}(f))^{1/2} \tag{4}$$

$$\gamma^2(f) = |R(f)|^2 \tag{5}$$

where, in Eq. (3), σ_{12} is the cross-covariance function of phase lag τ, and σ_{11} and σ_{22} are the variances of the two time series; and in Eqs. (4) and (5), f is the frequency, $S_{12}(f)$ the cross-power spectrum between the two time series, and $S_{11}(f)$ and $S_{22}(f)$ the auto-power window spectrum technique of Thomason (1982) is employed in the calculations of power spectrum, with application of the Fourier transform.

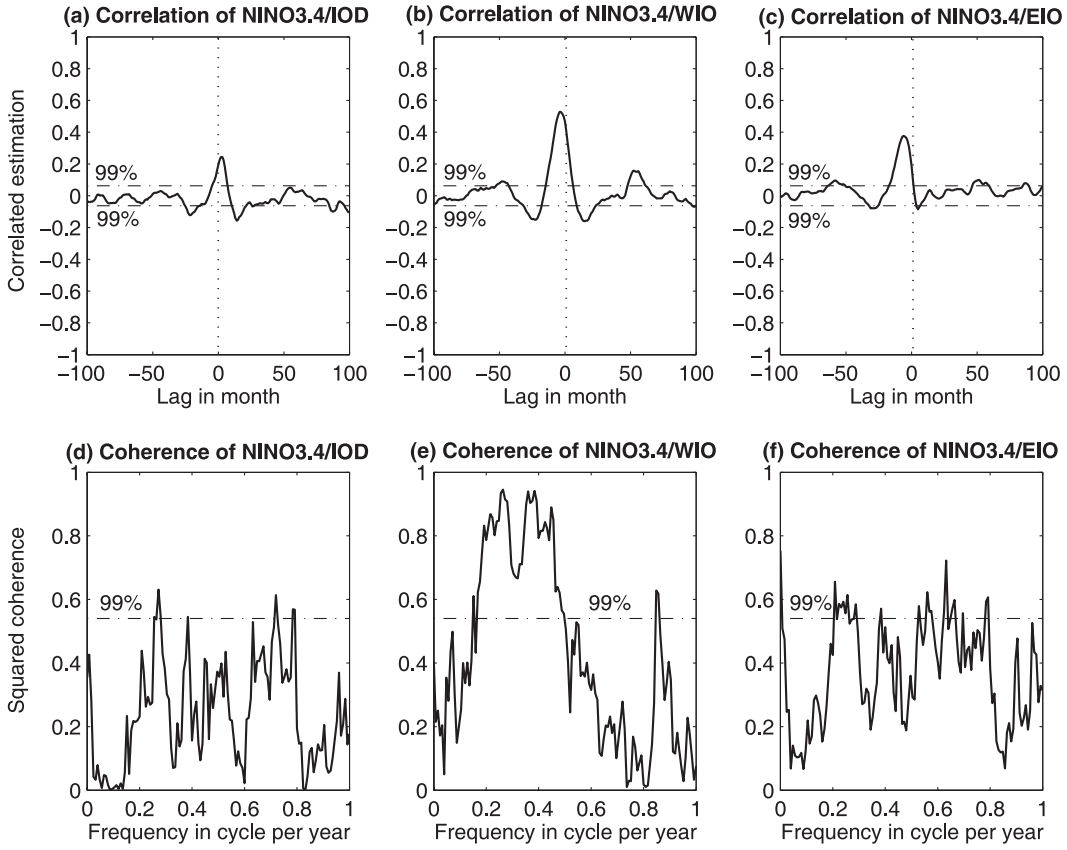

Fig. 2. Estimated cross-correlation (upper panels) and squared coherence (lower panels) between Niño-3.4 SST and Indian Ocean SSTs. Values of negative (positive) lags shown in the x-coordinate of each panel represent the correlations in which Niño-3.4 SST leads (lags) the Indian Ocean SSTs. Dashed lines show the threshold values of the significant test (assessed two-sided) at the 99% confidence level.

Figure 2 shows the cross-correlation and cross-coherence, calculated by Eqs. (3)–(5), between Niño-3.4 SST and the various IO SST indices. In the calculations, the seasonal cycles have been removed from the time series. The constant and linear trend terms have also been removed to meet the principle of statistics for correlation and coherence computations. Simultaneously, the Niño-3.4 SST is significantly related to the IO SSTs, especially the WIO SST, at the confidence level $\alpha = 0.99$ determined by the Monte Carlo test (Zhou and Zheng, 1999). However, the most significant correlation occurs when Niño-3.4 SST leads WIO SST by four months ($R = 0.53$ for the period of 1880–2004). The strongest relationship between Niño-3.4 SST and IOD appears when IOD leads by three months ($R = 0.24$) and the strongest relationship between Niño-3.4 and EIO SSTs appears when Niño-3.4 SST leads by six months ($R = 0.38$).

Figures 2d–f illustrate the Indo-Pacific SST relationship, measured by coherence, as a function of frequency bands. A very strong relationship is seen between Niño-3.4 and WIO SSTs on timescales of two to seven years, and of 14 months. A strong relationship is also found between Niño-3.4 and EIO SSTs in most of the frequency bands in the range from 15 months to five years. Relatively, the relationship between Niño-3.4 SST and IOD is less significant except on timescales of around 4.5 years and of 15–19 months.

The cross-correlation and cross-coherence between the various IO SST indices are displayed in Fig. 3. As expected, the IOD is significantly correlated with both WIO SST ($R = 0.48$) and EIO SST ($R = -0.67$). However, the maximum correlation between WIO and EIO SSTs occurs when the WIO SST leads by three months ($R = 0.36$), although the simultaneous correlation between the two is also significant. It can be seen from Figs. 2d–f that the IOD is strongly related with WIO and EIO SSTs in a wide range of frequency bands. In particular, the relationship between IOD and the EIO SST is especially strong on quasi-biennial (1.5–2.5 years) and near-annual timescales. However, a significant relationship between the WIO and EIO

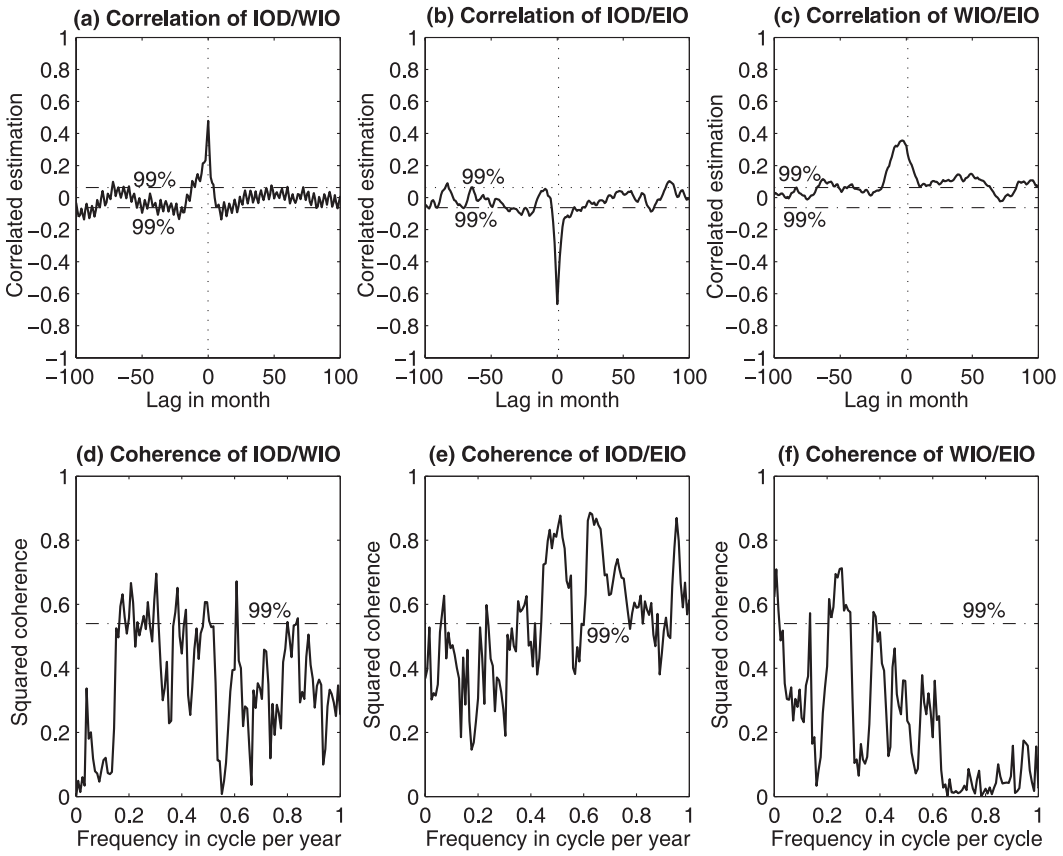

Fig. 3. Estimated cross-correlation (upper panels) and squared coherence (lower panels) between the various Indian Ocean SST indices. Values of negative (positive) lags shown in the x-coordinate represent the correlations in which the first index leads (lags) the second index indicated in the subtitle of each panel. Dashed lines show the threshold values of the significant test (assessed two-sided) at the 99% confidence level.

SSTs mainly appears on the timescales of four and 2.5 years. Indeed, the relationship between the two poles of IOD is very weak on quasi-biennial and higher timescales. This feature can be seen more thoroughly in Fig. 5.

Note that the above estimates are only about the mean features of the time span and frequency domain. We further depict the stability and variability of these features in specific frequency bands with respect to time processes by applying a technique in which a moving window is used. In this method, the coherence in time-frequency domains is derived first by estimating the values of a sub-series of 10 years and then by moving the data points successively for subsequent estimations. Figure 4 shows the distributions of coherence between Niño-3.4 SST and different IO SST indices in both time and frequency domains. The Niño-3.4 SST is most strongly related to WIO SST, and then to EIO SST, and the relationship between Niño-3.4 SST and IOD is the weakest, consistent with the features shown in Fig. 2. A highly significant relationship between Niño-3.4 and WIO SSTs exists on biennial and inter-annual timescales, especially in the late 1800s, during 1928–1957 and 1963–1988, and since 1993. A strong relationship between Niño-3.4 and EIO SSTs also appears in relatively higher frequencies from 1963–1978, and since 1990. The significant relationships between Niño-3.4 SST and IOD in inter-annual frequency bands during the 1960s–80s, and during the 1990s (see Fig. 4a) are, respectively, consistent with the results of Ashok et al., (2003b, Fig. 8c) and Saji and Yamagata (2003b, Fig. 11a).

It can be seen by comparing Fig. 5a with Fig. 5b that IOD is almost always more strongly linked to EIO SST than to WIO SST (refer to the significance levels to the right of the figure). Overall, the coherence between IOD and EIO SST is large in a wide range of frequency bands, from intra-seasonal to inter-annual, and the coherence between IOD and WIO SST is most significant near the intra-seasonal band, a feature that has not been shown in Fig. 3. Figure 5a also reveals an unstable IOD-WIO relationship with time, in contrast

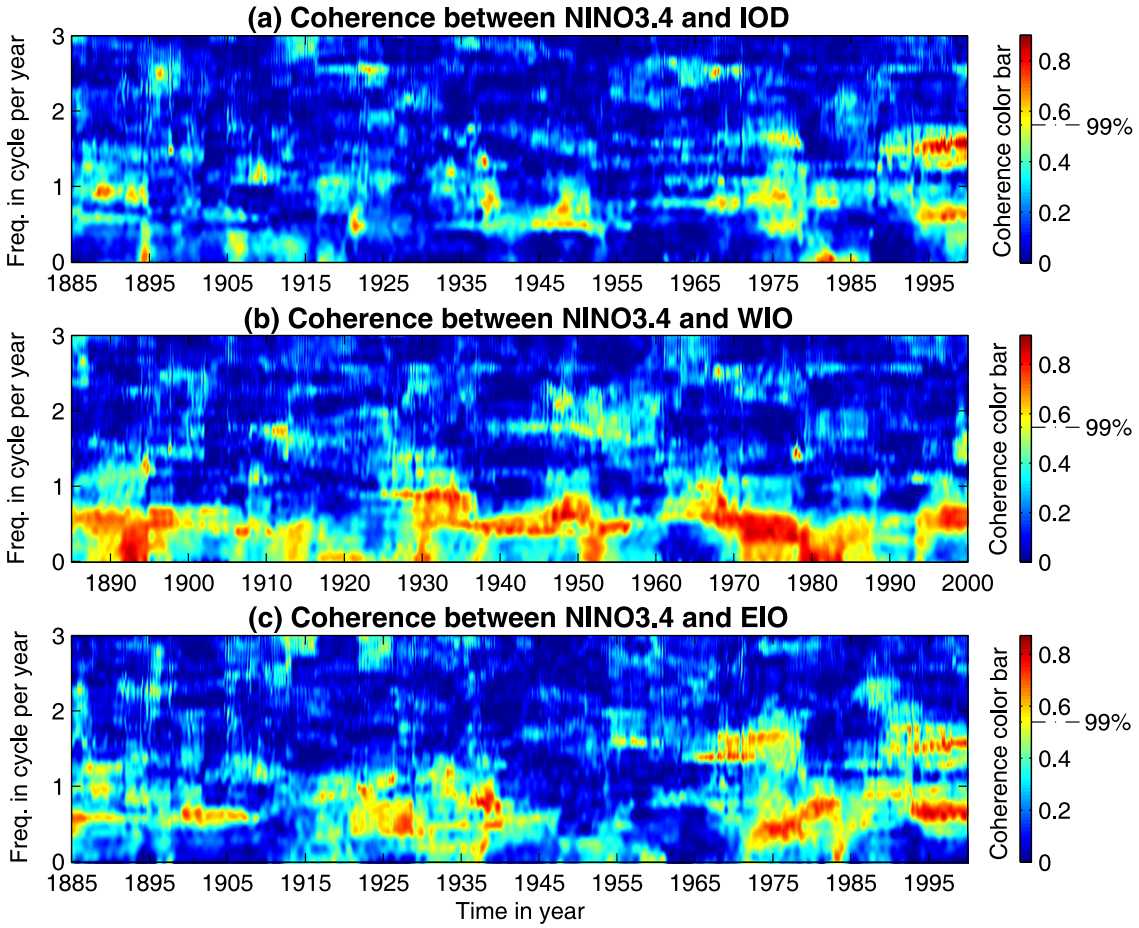

Fig. 4. Time-frequency distributions of monthly coherence (a) between Niño-3.4 SST and IOD, (b) between Niño-3.4 and WIO SSTs, and (c) between Niño-3.4 and EIO SSTs. The threshold value of the significant test at the 99% confidence level is given by the dashed-dotted lines in the color bars on the right-hand side of the figure.

to the more stable IOD-EIO relationship shown in Fig. 5b. It is interesting to note that strong relationships between IOD and EIO SST often appear when weak relationships occur between IOD and WIO SST, especially during 1915–55, and in the 1990s.

Surprisingly, the relationship between WIO and EIO SSTs (Fig. 5c) is much weaker than the relationship between IOD and WIO SST, and that between IOD and EIO SST, even though the IOD is defined by the variability of WIO and EIO SSTs. For the relatively strong relationship in the low frequency bands, inter-decadal variability is evident, and thus the relationship is unstable.

5. Seasonality of the relationships between various SST indices

Since the variability of Indo-Pacific SSTs is characterized by strong seasonal cycles, it is important to depict the seasonality of the above-addressed features. Figure 6 presents the correlation and coherence between Niño-3.4 SST and different IO SST indices for the various seasons. It can be seen from Fig. 6a that the Niño-3.4 SST has the strongest relationship with IOD in September-October-November (SON, $R = 0.51$), confirming the results of previous studies. This strong relationship occurs mainly on 3- to 4.5-year timescales (see the coherence panels). The Niño-3.4 SST, which shows no significant relationships with IOD in March-April-May (MAM) and December-January-February (DJF), is also moderately significantly related to IOD in JJA ($R = 0.33$), mainly on four-year and shorter timescales. The relationships between Niño-3.4 and WIO SSTs are significant in all seasons, especially in DJF ($R = 0.60$) and MAM ($R = 0.59$), and the strong relationships appear over a wide range of inter-annual timescales (Fig. 6b). As seen from Fig. 6c, there exists strong inter-

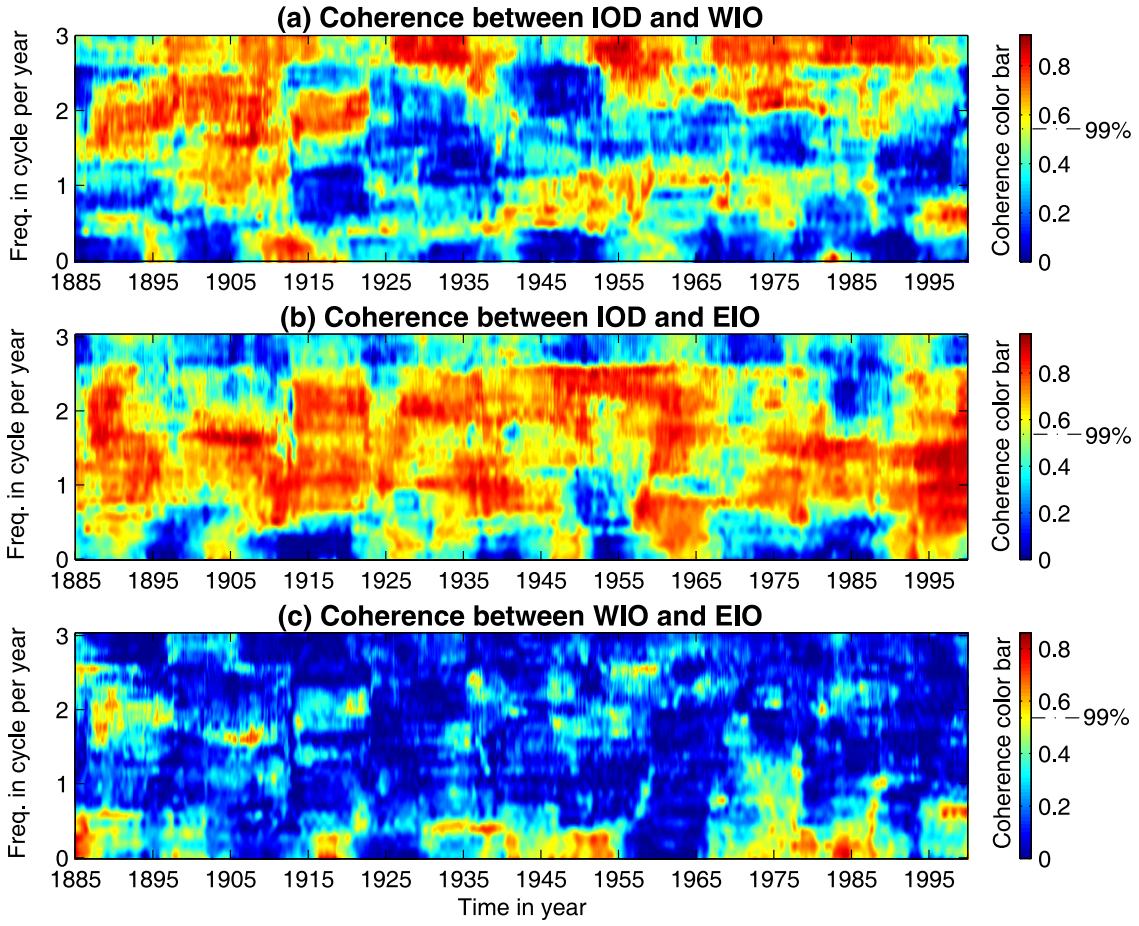

Fig. 5. (a) Time-frequency distributions of monthly coherence between IOD and WIO SST, (b) between IOD and EIO SST, and (c) between WIO and EIO SSTs. The threshold value of the significant test at the 99% confidence level is given by the dashed-dotted lines in the color bars on the right-hand side of the figure.

annual Niño-3.4-EIO relationships in DJF ($R = 0.56$) and MAM ($R = 0.55$), but there are no significant simultaneous relationships between the two in JJA and SON. It is impressive that the Niño-3.4 SST is correlated with both WIO and EIO SSTs positively in MAM and DJF. This feature will be seen again later in Fig. 7c.

Figure 7 shows that while the IOD is significantly correlated to WIO SST only in SON ($R = 0.67$) and June-July-August (JJA; $R = 0.56$; Fig. 7a), it is strongly and negatively related to EIO SST in all seasons, especially in SON ($R = -0.73$) and JJA ($R = -0.69$; Fig. 7b). More strikingly, although the IOD is defined based on the WIO and EIO SSTs and it is more prominent in JJA and SON than other seasons, insignificant WIO-EIO correlation appears in JJA ($R = 0.19$) and SON ($R = 0.0$), as seen from Fig. 7c. On the contrary, strong correlation appears in MAM, ($R = 0.64$) and DJF, ($R = 0.72$) when the IOD generally disappears. It is also noted that the WIO and EIO SSTs are strongly and positively correlated in both DJF and MAM, which leads to a positive correlation ($R = 0.32$) between the whole month values of the two, consistent with the positive Niño-3.4-WIO relationship and Niño-3.4-EIO relationship in these two seasons shown in Figs. 6b and 6c. However, this positive relationship became weaker ($R = 0.19$) during the period of 1958–2004.

Figure 7a also shows that the strong IOD-WIO relationship in SON mainly occurs on six-year and shorter timescales (see the coherence panels). In JJA, large coherence between the two occurs on the timescales of 2.5 to eight years. Large IOD-EIO coherence in JJA and SON appears in wider frequency bands than that in MAM and DJF (Fig. 7b). Furthermore, in DJF, WIO SST is significantly related to EIO SST on around 2.5 and 4.5 years and longer timescales (Fig. 7c). Note that the relationships revealed for very low timescales are generally less reliable than the others and thus are not discussed in detail here.

Table 2. Maximum correlation of seasonal SSTs between Niño-3.4/IOD, Niño-3.4/WIO, Niño-3.4/EIO, IOD/WIO, IOD/EIO, and WIO/EIO. The numbers in the second column for each season represent the number of months that the first index of each pair (see the column) leads the second index. Significant values at the 99% confidence level are emboldened.

	MAM		JJA		SON		DJF	
	Correlation	Lag (yr)	Correlation	Lag (yr)	Correlation	Lag (yr)	Correlation	Lag (yr)
Niño-3.4/IOD	−0.13	0	**0.33**	0	**0.51**	0	−0.11	1
Niño-3.4/WIO	**0.59**	0	**0.33**	0	**0.55**	0	**0.60**	0
Niño-3.4/EIO	**0.55**	0	−0.11(**0.41**)	0(1)	−0.2(**0.30**)	0(1)	**0.56**	0
IOD/WIO	−0.16	2	**0.56**	0	**0.67**	0	0.19	0
IOD/EIO	**− 0.66**	0	**−0.69**	0	**−0.73**	0	**−0.53**	0
WIO/EIO	**0.64**	0	0.19(**0.29**)	0(1)	0.0(**0.41**)	0(1)	**0.72**	0

Table 2 summarizes the main features of seasonality of the relationships between Indo-Pacific SSTs. It shows the maximum values from both simultaneous and lag correlations for each season. Besides those discussed previously for Figs. 6 and 7, several additional features should be pointed out. First, for JJA and SON, although the simultaneous correlation between Niño-3.4 and EIO SSTs is weak, a significant relationship appears when Niño-3.4 SST leads by a year (see row five). Second, also for these two seasons, significant correlation occurs between WIO and EIO SSTs ($R = 0.29$ for JJA, and $R = 0.41$ for SON) when the WIO SST leads by a year, although the simultaneous correlation between the two is apparently insignificant.

We further examine the one-point correlation patterns of IOD and Niño-3.4 SST. It can be seen from Fig. 8 that the Niño-3.4 SST links significantly to many features in IO and the western-central Pacific (Considering that the quality of grid-point data in the early decades may not be reliable for this type of computations, we only analyze the period of 1950–2005. However, an examination of the patterns for 1880–2005 reveals similar features.) The well known features include the positive correlation in IO and the negative correlation in the western Pacific Ocean. However, in both JJA and SON (Figs. 8g and 8h), the area of negative correlation extends westward to the eastern IO. This feature can also be rephrased as a westward retreat of the positive correlation zone of IO, emphasizing the IOD structure in these two seasons. A comparison between the left column and the right column of the figure indicates that the IOD and Niño-3.4 SST are associated with similar features of the Indo-Pacific SSTs in JJA and SON. Given the weak relationship between WIO and EIO SSTs and the strong relationship between IOD and Niño-3.4 SST (see Table 2), the similarity between Figs. 8c–d and Figs. 8g–h is unfavorable for claiming an independence of IOD from the Niño-3.4 SST for these two seasons. Note that the significant and opposite correlations appearing between the western and eastern IO in Figs. 8c and 8d, for JJA and SON, result from the definition of IOD. The correlation pattern itself does not imply significant negative correlations between the WIO and EIO SSTs, both of which are part of IOD used in the computations. Thus, the feature shown here does not contradict the features presented in Figs. 5c and 7c. In DJF (Figs. 8a and 8b) and MAM (Figs. 8e and f), the IOD and Niño-3.4 SST are linked to completely different SST variations. Although the WIO and EIO SSTs are strongly (but positively) correlated (see Fig. 7c), IOD is unimportantly weak and even disappears in these seasons when uniform warming or cooling, the most dominant mode of IO SST and usually associated with ENSO, exerts a large impact on the climate (Yoo et al., 2006).

Figure 9 shows the lag correlation patterns of IOD and Niño-3.4 SST in which these indices lead the grid-point SSTs by one season. For the Niño-3.4 SST related features (right column), the lag correlation patterns are similar to the simultaneous correlation patterns shown in Figs. 8e–h due to the persistence of Niño-3.4 SST from one season to the next. Relatively large differences appear between Figs. 8g and 9g because of the drop in memory of the spring SST (Webster and Yang, 1992).

For the Indian Ocean, there exists similar features between Figs 9a and 9e. Because of the difference between Fig. 8a and Fig. 8e (for DJF) and because of the strong IOD-Niño-3.4 relationship in SON (see Table 2), these similar features can be attributed largely to the Pacific impact, consistent to many previous studies. The difference between Fig. 9b and Fig. 9f is related to the insignificant relationships between IOD and Niño-3.4 SST in both DJF and MAM, as shown in Table 2. A similar analysis indicates that the resemblance between Fig. 9d and Fig. 9h is due to the strong relationships between IOD and Niño-3.4 SST in both JJA and SON. Finally, the difference between Fig. 9c and Fig. 9g is in contrast to the similarity between Fig. 8c and Fig. 8g because the IOD-Niño-3.4

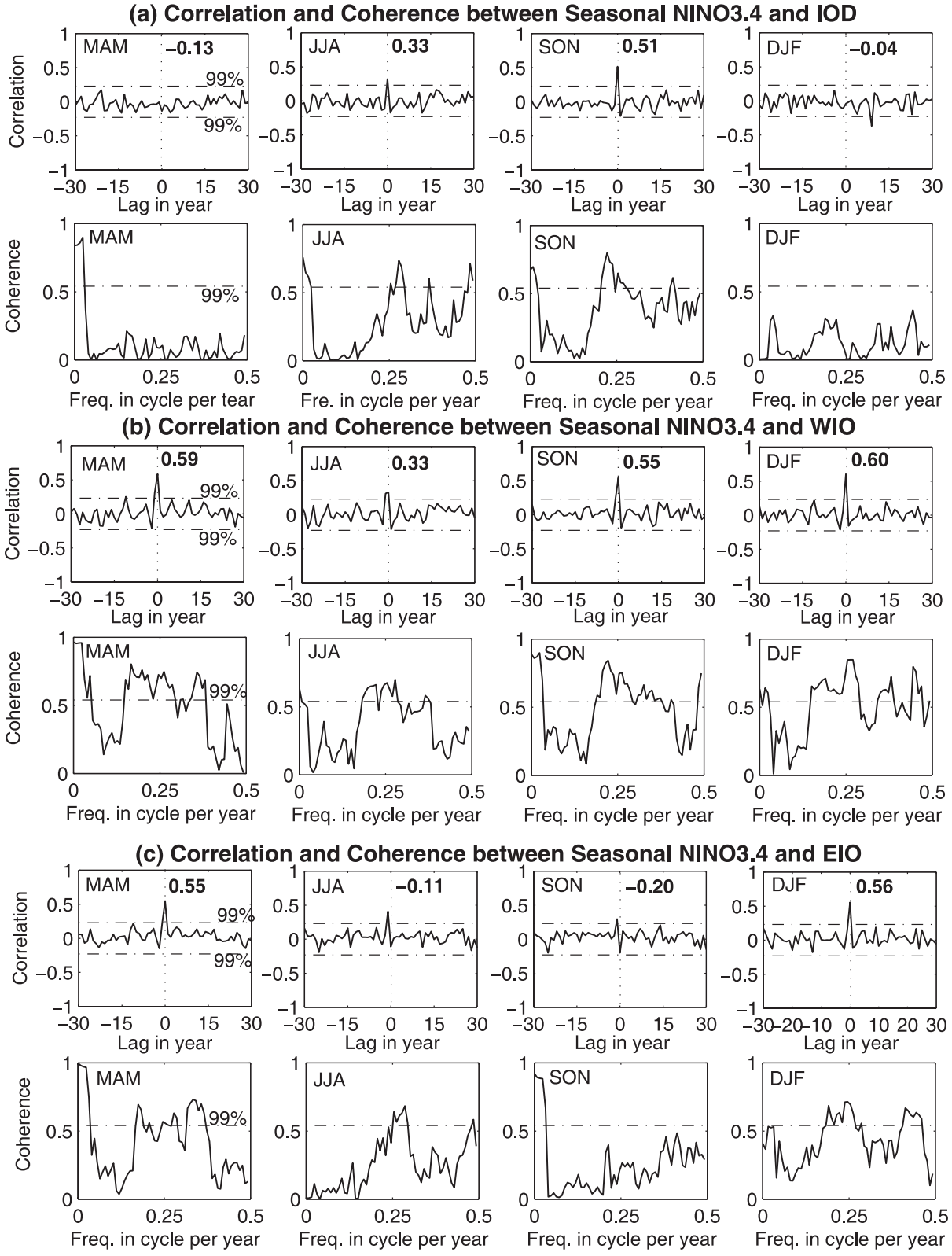

Fig. 6. Correlation and coherence (a) between Niño-3.4 SST and IOD, (b) between Niño-3.4 and WIO SSTs, and (c) between Niño-3.4 and EIO SSTs. Results are shown for MAM, JJA, SON, and DJF, respectively, from the left panels to the right panels. The numbers shown in the correlation panels are correlation coefficients.

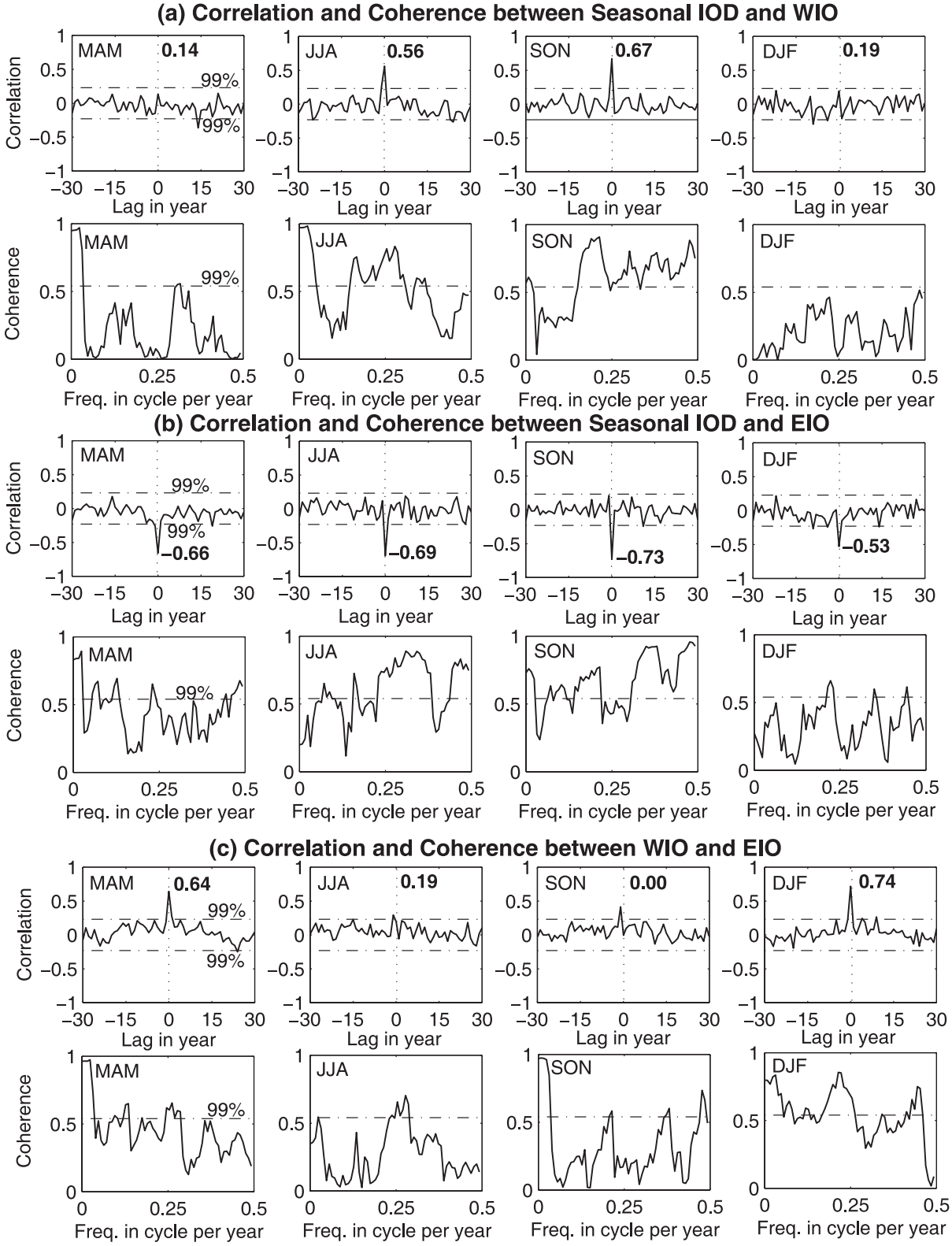

Fig. 7. Correlation and coherence (a) between IOD and WIO SST, (b) between IOD and EIO SST, and (c) between WIO and EIO SSTs. Results are shown for MAM, JJA, SON, and DJF, respectively, from the left panels to the right panels. The numbers shown in the correlation panels are correlation coefficients.

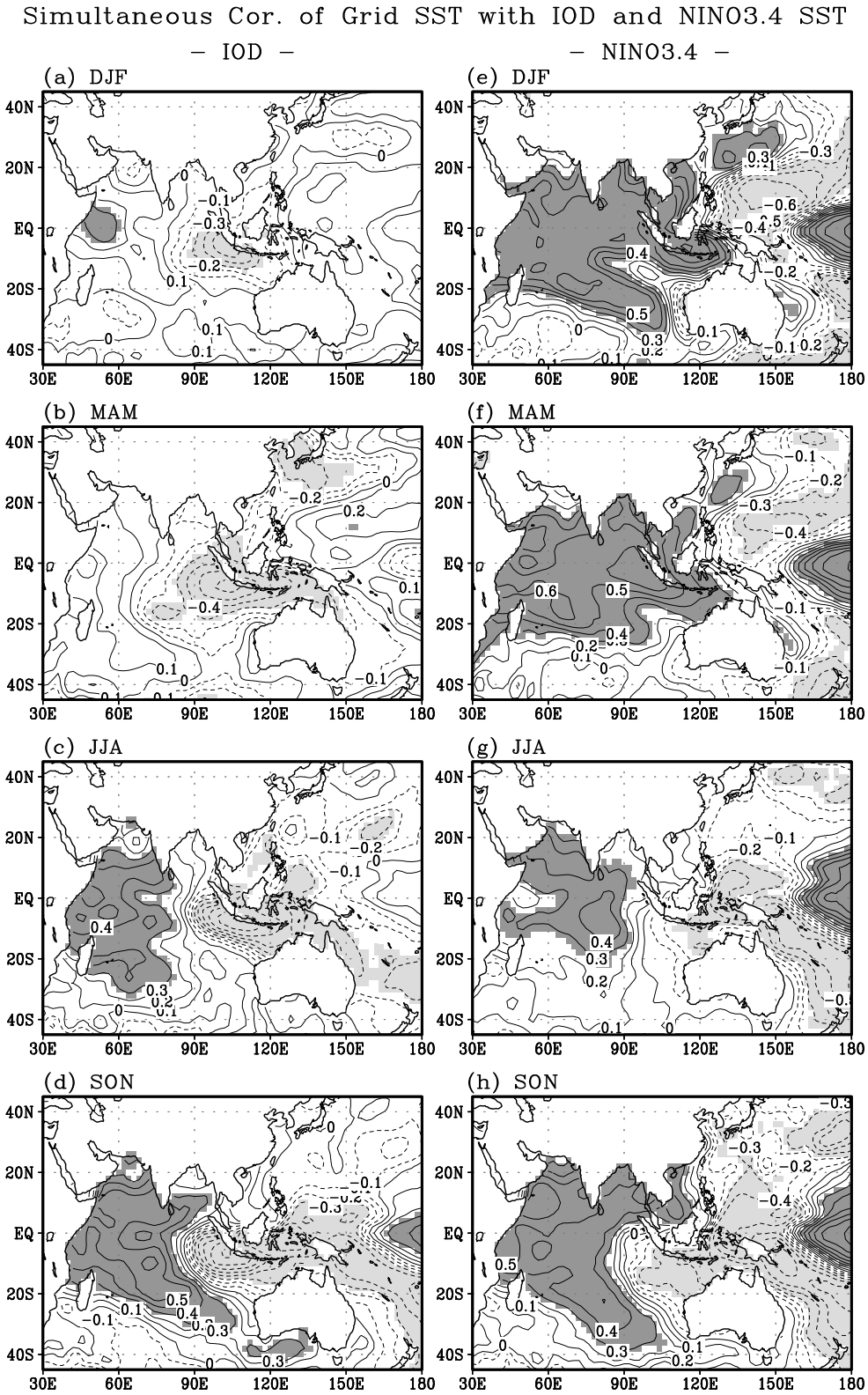

Fig. 8. Patterns of simultaneous correlations (1950–2005) (a–d) between IOD and grid-point SST and (e–h) between Niño-3.4 SST and grid-point SST for each season. Significant values exceeding the 95% confidence level are shaded.

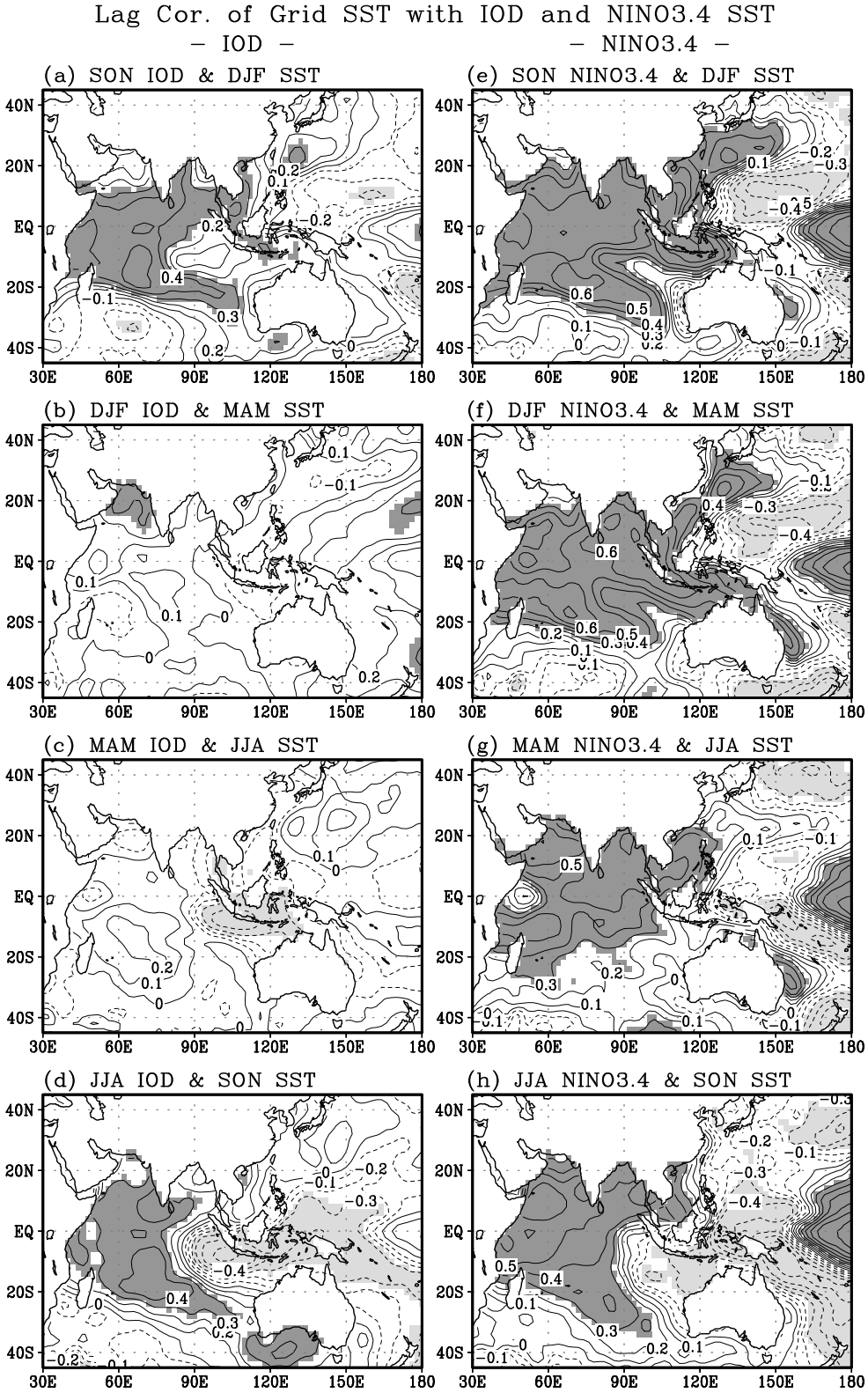

Fig. 9. Patterns of seasonal lag correlations (1950–2005) (a–d) between IOD and subsequent grid-point SST and (e–h) between Niño-3.4 SST and subsequent grid-point SST. Significant values exceeding the 95% confidence level are shaded.

relationship is weak in MAM but strong in JJA. A careful examination reveals a weak similarity in IO, between Fig. 8c and Fig. 9c, in terms of the sign of correlation, reflecting a certain relationship in IOD from MAM, when the IOD is about to develop, to JJA.

6. Summary and discussion

We have depicted the seasonally-dependent features of the structural change of IOD and the relationships between Niño-3.4 SST, IOD, and WIO and EIO SSTs, with a focus on the distributions of these features in both time and frequency domains. The WOI SST has the largest amplitudes in annual and semiannual oscillations, and the semiannual oscillation of IOD is even stronger than its annual oscillation. In all IO SST indices, the nonseasonal signals are weaker than the seasonal signal by about an order of magnitude. On the other hand, the Niño-3.4 SST has large inter-annual variability that is only second to its annual variability. The IOD is strongly and stably related to EIO SST in a wide range of frequency bands and in all seasons, but it is less significantly related to WIO SST in the boreal winter and spring. There exists a generally weak and unstable relationship between WIO and EIO SSTs, especially in the biennial and higher frequency bands. The Niño-3.4 SST has a strong positive relationship with WIO SST in all seasons, mainly in the biennial and lower frequency bands. However, it shows no significant relationship with EIO SST in summer and fall and with IOD SST in winter and spring.

This study reveals a robust feature: the WIO SST is correlated with EIO SST insignificantly in boreal summer and fall, but highly significantly and positively in winter and fall. This feature presents a caution in the definition and application of IOD because the phenomenon, defined based on the WIO and EIO SSTs, is only apparent in summer and fall but is unimportantly weak and even disappears in winter and spring. Consistent with the above feature, the Niño-3.4 SST is significantly and positively related to both WIO and EIO SSTs in winter and spring.

Acknowledgements. The authors thank Prof. Li Chongyin and Drs. Huang Bohua, Xue Yan, and Zhang Qin for their constructive comments on an earlier version of the manuscript.

REFERENCES

Ailikun, B., and T. Yasunari, 2001: ENSO and Asian summer monsoon: Persistence and transitivity in the seasonal march. *J. Meteor. Soc. Japan*, **79**, 145–159.

Ashok, K., Z. Guan, and T. Yamagata, 2001: Impact of the Indian Ocean dipole on the decadal relationship between the Indian monsoon rainfall and ENSO. *Geophys. Res. Lett.*, **28**, 4499–4502.

Ashok, K., Z. Guan, and T. Yamagata, 2003a: Influence of the Indian Ocean dipole on the Australian winter rainfall. *Geophys. Res. Lett.*, **30**, doi: 10.1029/2003GL017926.

Ashok, K., Z. Guan, and T. Yamagata, 2003b: A look at the relationship between the ENSO and the Indian Ocean dipole. *J. Meteor. Soc. Japan*, **81**, 41–56.

Ashok, K., Z. Guan, N. H. Saji, and T. Yamagata, 2004: Individual and combined influences of ENSO and the Indian Ocean dipole on the Indian summer monsoon. *J. Climate*, **17**, 3141–3155.

Behera, S. K., and T. Yamagata, 2003: Influence of the Indian Ocean Dipole on the Southern Oscillation. *J. Meteor. Soc. Japan*, **81**, 169–177.

Behera, S. K., S. Krishnan, and T. Yamagata, 1999: Unusual ocean-atmosphere conditions in the tropical Indian Ocean during 1994. *Geophys. Res. Lett.*, **26**, 3001–3004.

Black, E., 2005: The relationship between Indian Ocean sea surface temperature and east African rainfall. *Phil. Trans. Roy. Soc. London*, **363**, 43–47.

Black, E., J. Slingo, and K. R. Sperber, 2003: An observational study of the relationship between excessively strong short rains in coastal East Africa and Indian Ocean SST. *Mon. Wea. Rev.*, **131**, 74–94.

Chao Jiping, Chao Qingchen and Liu Lin, , 2005: The ENSO events in the tropical Pacific and dipole events in the Indian Ocean. *Acta Meteorologica Sinica*, **63**, 594–602. (in Chinese)

Ding, X., D. Zheng, and S. Yang, 2002: Variations of the surface temperature in Hong Kong during the last century. *International Journal of Climatology*, **22**, 715–730.

Gadgil, S, and S. Sajani, 1998: Monsoon prediction in the AMIP runs. *Climate Dyn.*, **14**, 659–689.

Guan, Z., and T. Yamagata, 2003: The unusual summer of 1994 in East Asia: IOD teleconnections. *Geophys. Res. Lett.*, **30**, doi:10.1029/2002GL016831.

Huang, B., and J. L. Kinter III, 2002: The interannual variability in the tropical Indian Ocean. *J. Geophys. Res.*, **107**, 3199, doi: 10:1029/2001JC001278.

Huang, R., W. Chen, B. Yang, and R. Zhang, 2004: Recent advances in studies of the interaction between the East Asian winter and summer monsoons and ENSO cycle. *Adv. Atmos. Sci.*, **21**, 407–424.

Jenkins, G., and D. Watts, 1968: *Spectrum Analysis and Its Applications*. Holden-Day, San Francisco, CA, 525pp.

Ju, J., and J. Slingo, 1995: The Asian summer monsoon and ENSO. *Quart. J. Roy. Meteor. Soc.*, **121**, 1133–1168.

Lau, K.-M., and H.-T. Wu, 2001: Principal modes of rainfall-SST variability of the Asian summer monsoon: A reassessment of the monsoon-ENSO relationship. *J. Climate*, **14**, 2880–2895.

Lau, N.-C., and B. Wang, 2006: Interactions between the Asian monsoon and the El Niño/Southern Oscillation. *The Asian Monsoon*, B. Wang, Ed., Praxis Publishing Ltd, Chichester, UK, 479–512.

Li, C., and M. Mu, 2001a: Influence of the Indian Ocean dipole on Asian monsoon circulation. *Exchanges*, **6**, 11–14.

Li, C., and M. Mu, 2001b: The influence of the Indian Ocean dipole on atmospheric circulation and climate. *Adv. Atmos. Sci.*, **18**, 831–843.

Li Chongyin, Mu Mingquan, and Pan Jing, 2002a: Indian Ocean temperature dipole and SSTA in the equatorial Pacific Ocean. *Chinese Science Bulletin*, **47**, 236–239.

Li, T., Y. Zhang, E. Lu, and D. Wang, 2002b: Relative role of dynamic and thermodynamic processes in the development of the Indian Ocean dipole: An OGCM diagnosis. *Geophys. Res. Lett.*, **29**, 2110, doi: 10.1029/2002GL015789.

Li, T., B. Wang, C.-P. Chang, and Y. Zhang, 2003: A theory for the Indian Ocean dipole-zonal mode. *J. Atmos. Sci.*, **60**, 2119–2135.

Loschnigg, J., G. A. Meehl, P. J. Webster, J. M. Arblaster, and G. P. Compo, 2003: The Asian monsoon, the tropospheric biennial oscillation, and the Indian Ocean zonal mode in the NCAR GCM. *J. Climate*, **16**, 1617–1642.

Meehl, G. A., J. M. Arblaster, and J. Loschnigg, 2003: Coupled ocean-atmosphere dynamical processes in the tropical Indian and Pacific Oceans and the TBO. *J. Climate*, **16**, 2138–2158.

Morlet, J., G. Arehs, I. Fourgeau, and D. Giard, 1982: Wave propagation and sampling theory. *Geophysics*, **47**, 203–221.

Powell, M., and J. Reid, 1969: On applying Householder's method to linear least squares problem. Proce. *IFIP Congress 1968*, A. Morell, Ed., North-Holland, Amsterdam, 122–126.

Rao, S. A., and S. K. Behera, 2005: Subsurface influence on SST in the tropical Indian Ocean: Structure and interannual variability. *Dyn. Atmos. Oceans*, **39**, 103–135.

Rasmusson, E. M., and T. H. Carpenter, 1982: Variations in tropical sea surface temperature and surface wind fields associated with the Southern Oscillation/El Niño. *Mon. Wea. Rev.*, **110**, 354–384.

Rasmusson, E. M., and T. H. Carpenter, 1983: The relationship between eastern equatorial Pacific sea surface temperatures and rainfall over India and Sri Lanka. *Mon. Wea. Rev.*, **111**, 517–528.

Ropelewski, C. F., and M. S. Halpert, 1987: Global and regional scale precipitation patterns associated with the El Niño/Southern Oscillation. *Mon. Wea. Rev.*, **115**, 1606–1626.

Saji, N. H., and T. Yamagata, 2003a: Possible impacts of Indian Ocean dipole mode events on global climate. *Climate Research*, **25**, 151–169.

Saji, N. H., and T. Yamagata, 2003b: Structure of SST and surface wind variability during Indian Ocean dipole mode events: COADS observations. *J. Climate*, **16**, 2735–2751.

Saji, N. H., B. N. Goswami, P. N., Vinayachandran, and T. Yamagata, 1999: A dipole mode in the tropical Indian Ocean. *Nature*, **401**, 360–363.

Saji, N. H., T. Ambrizzi, and S. E. T. Ferraz, 2005: Indian Ocean Dipole mode events and austral surface temperature anomalies. *Dyn. Atmos. Oceans*, **39**, 87–101.

Smith, T. M., and R. W. Reynolds, 2003: Extended reconstruction of global sea surface temperatures based on COADS data (1854–1997). *J. Climate*, **16**, 1495–1510.

Thomason, D., 1982: Spectrum estimation and harmonic analysis. *Institute of Electrical and Electronics Engineers Proc.*, **70**, 1055–1096.

Wang, B., R. Wu, and X. Fu, 2000: Pacific-East Asian teleconnection: How does ENSO affect East Asian climate? *J. Climate*, **13**, 1517–1536.

Webster, P. J., and S. Yang, 1992: Monsoon and ENSO: Selectively interactive systems. *Quart. J. Roy. Meteor. Soc.*, **118**, 877–926.

Webster, P. J., A. M. Moore, J. P. Loschnigg, and R. R. Leben, 1999: Coupled ocean-atmosphere dynamics in the Indian Ocean during 1997–98. *Nature*, **401**, 356–360.

Wu, R., and B. P. Kirtman, 2004: Impacts of the Indian Ocean on the Indian summer monsoon-ENSO relationship. *J. Climate*, **17**, 3037–3054.

Yan, X., T. M. Smith, and R. W. Reynolds, 2003: Interdecadal changes of 30-yr SST normals during 1871–2000. *J. Climate*, **16**, 1601–1612.

Yang, H., and C. Li, 2005: The influence of tropical Pacific-Indian Ocean associated mode on South-Asia high. *Chinese J. Atmos. Sci.*, **29**, 99–110.

Yang, S., and K.-M. Lau, 2006: Interannual variability of the Asian monsoon. *The Asian Monsoon*, B. Wang, Ed., Praxis Publishing Ltd, Chichester, UK, 259–293.

Yang, S., X. Ding, D. Zheng, and Q. Li, 2007: Depiction of the variability of Great Plains precipitation and its relationship with the tropical central-eastern Pacific SST. *J. Appl. Meteor. Climatol.*, **46**, 136–153.

Yoo, S.-H., S. Yang, and C.-H. Ho, 2006: Variability of the Indian Ocean sea surface temperature and its impacts on Asian-Australian monsoon climate. *J. Geophys. Res.*, **111**, D03108, doi: 10.1029/2005JD006001.

Yu, J.-Y., S.-P. Weng, and J. D. Farrara, 2003: Ocean roles in the TBO transitions of the Indian-Australian monsoon system. *J. Climate*, **16**, 3072–3080.

Yulaeva, E., and J. M. Wallace, 1994: Signature of ENSO in global temperature and precipitation fields derived from the microwave sounding unit. *J. Climate*, **7**, 1719–1736.

Zhang, Q., and S. Yang, 2007: Seasonal phase-locking of the peak events in eastern Indian Ocean. *Adv. Atmos. Sci.* (in press)

Zhang, R., A. Sumi, and M. Kimoto, 1999: A diagnostic

study of the impact of El Niño on the precipitation in China. *Adv. Atmos. Sci.*, **16**, 229–241.

Zheng, D. W., B. F. Chao, Y. H. Zhou, and N. H. Yu, 2000: Improvement of edge effect of the wavelet time-frequency spectrum: Application to the length of day series. *J. Geodesy*, **74**, 249–254.

Zhou Yonghong, and Zheng Dawei, 1999: Monte Carlo simulation test of correlation significance levels. *Acta Geodaetica et Cartographica Sinica*, **22**, 313–318. (in Chinese)